12-11-2014

Comparison on Different Discrete Fractional Fourier Transform (DFRFT) Approaches

Bal Santhanam

DEPARTMENT OF ELECTRICAL AND COMPUTER ENGINEERING

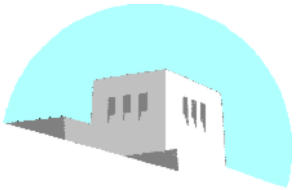

SCHOOL OF ENGINEERING
UNIVERSITY OF NEW MEXICO

Comparison on Different Discrete Fractional Fourier Transform (DFRFT) Approaches

Balu Santhanam and Ishwor Bhatta
Department of Electrical & Computer Engineering
University of New Mexico, Albuquerque, NM: 87131
Tel: 505 277-1611, Fax: 505 277 1439
Email: bsanthan@unm.edu, ibhatta@unm.edu

UNM Technical Report: EECE-TR-14-02

Report Date: December 8, 2014

Abstract

As an extension of the conventional Fourier transform and as a time-frequency signal analysis tool, the fractional Fourier transforms (FRFT) are suitable for dealing with various types of non-stationary signals. Taking advantage of the properties and non-stationary features of linear chirp signals in the Fourier transform domain, several methods of extraction and parameter estimation for chirp signals are proposed, and a comparative study has been done on chirp signal estimation. Computation of the discrete fractional Fourier transform (DFRFT) and its chirp concentration properties are both dependent on the basis of DFT eigenvectors used in the computation. Several DFT-eigenvector bases have been proposed for the transform, and there is no common framework for comparing them. In this report, we compare several different approaches from a conceptual viewpoint and review the differences between them. We discuss five different approaches, namely: (1) the bilinear transformation method, (2) the Grunbaum method, (3) the Dickenson-Steiglitz method, also known as the S-matrix method, (4) the quantum mechanics in finite dimension (QMFD) method, and (5) the higher order S-matrix method, to find centered-DFT (CDFT) commuting matrices and the various properties of these commuting matrices. We study the properties of the eigenvalues and eigenvectors of these commuting matrices to determine whether they resemble those of corresponding continuous Gauss-Hermite operator. We also measure the performance of these five approaches in terms of: mailobe-to-sidelobe ratio, 10-dB bandwidth, quality factor, linearity of eigenvalues, chirp parameter estimation error, and, finally peak-to-parameter mapping regions. We compare the five approaches using these performance metrics and point out that the modifiwd QMFD approach produces the best results in terms of bandwidth, invertibility of the peak-parameter mapping, linearity of the eigenvalue spectrum and parameter estimation error for chirp signal.

Keywords

Discrete fractional Fourier transform, linear chirp signal, chirp parameter estimation, parameter estimation error, peak-to-parameter mapping, invertibilty region.

1 Introduction

Pei, Hsue and Ding used the error-norm parameter to compare the eigenvectors of different DFT commuting matrices [1] to check the similarity between the eigenvector and the continuous G-H function. Serbes and Durak-Ata also used the same parameter for comparison in [2]. These analyses only determine how close the eigenvectors are to the sampled G-H function. As stated in [3], the linearity of the eigenvalue spectrum is another important parameter used to determine the closeness of the generating matrix to the G-H functions. Santhanam and Peacock introduced the valid mapping region criteria for peak-to-parameter mapping estimation [4]. In addition to the all the above mentioned parameters, we employed a few other parameters to find the best among the various CDFT commuting matrix approaches. In order to compare the different methods, we used the following performance metrics;

- Mainlobe-to-Sidelobe Ratio
- 10-dB Bandwidth
- Quality Factor
- Linearity of Eigenvalues
- Error-norm of the Eigenvectors
- Parameter Estimation Error
- Peak-to-Parameter Mapping Region

Using these seven parameters we seek to determine the best CDFT commuting matrix among the five different methods to be used in chirp signal applications. The five methods used for comparison in this paper are (1) the S-matrix method [5], (2) the Infinite order second derivative approximation method [1], (3) the bilinear transformation method [2], (4) the Quantum mechanics in finite dimension with modification (QMOD) [6] and (5) the Grunbaum method [7]. The eigenvectors of these commuting matrices are related to the continuous G-H function. Therefore, after this comparison we will be able to find the particular commuting matrix whose eigenvectors and eigenvalues are closest to those of the continuous G-H operator. In addition, the comparison will allow us to measure the quality of the peak that contains information regarding the chirp rate and center frequency parameters.

2 Computing the Discrete Fractional Fourier Transform

2.1 The Dickinson and Steiglitz (D-S) Method

Dickinson and Steiglitz defined a DFT commuting matrix [5], whose eigenvectors look like G-H function, as

$$\mathbf{S} = \begin{pmatrix} 2 & 1 & 0 & \dots & 0 & 1 \\ 1 & 2\cos\omega & 1 & \dots & 0 & 0 \\ \vdots & \vdots & \vdots & \ddots & \vdots & \vdots \\ 0 & 0 & 0 & \dots & 2\cos(N-2)\omega & 1 \\ 1 & 0 & 0 & \dots & 1 & 2\cos(N-1)\omega \end{pmatrix}, \tag{1}$$

where $\omega = \frac{2\pi}{N}$.

Here the diagonal elements are $2\cos(\frac{2\pi}{N}n)$, $0 \le n \le N-1$. This makes the matrix $\mathbf{S}$ commute with the DFT. If we change the range of n from $0 \le n \le N-1$ to $|n| \le \frac{N-1}{2}$, we will have a new $\mathbf{S}$-matrix which will commute with CDFT.

$$i.e.\ [\mathbf{W}, \mathbf{S}_{cen}] = \mathbf{W} * \mathbf{S}_{cen} - \mathbf{S}_{cen} * \mathbf{W} = 0, \tag{2}$$

where $\mathbf{W}$ is the Centered DFT and $\mathbf{S}_{cen}$ is the Centered version of S-matrix.

2.2 The Bilinear Transformation Method

Another approach to generating a DFT commuting matrix is introduced by Serbes and Durak-Ata in [2]. They defined a new DFT commuting matrix as;

$$\mathbf{B} = \mathbf{B}_1^{-1}\mathbf{E}_2 + \mathbf{W}\mathbf{B}_1^{-1}\mathbf{E}_2\mathbf{W}^{-1}, \tag{3}$$

where

$$\mathbf{B}_1 = \begin{bmatrix} k & 1 & 0 & \dots & \dots & 0 & 1 \\ 1 & k & 1 & \dots & \dots & 0 & 0 \\ 0 & 1 & k & \dots & \dots & \vdots & \vdots \\ \vdots & \vdots & \vdots & \ddots & \ddots & \vdots & \vdots \\ 1 & 0 & 0 & \dots & \dots & 1 & k \end{bmatrix}. \tag{4}$$

$$\mathbf{E}_2 = \begin{bmatrix} -2 & 1 & 0 & \dots & \dots & 0 & 1 \\ 1 & -2 & 1 & \dots & \dots & 0 & 0 \\ 0 & 1 & -2 & \dots & \dots & \vdots & \vdots \\ \vdots & \vdots & \vdots & \ddots & \ddots & \vdots & \vdots \\ 1 & 0 & 0 & \dots & \dots & 1 & -2 \end{bmatrix}. \tag{5}$$

W = DFT matrix and $k = 10^9$ is used in this thesis.

This newly generated matrix **B** commutes with DFT. In order to make it commute with the centered version of DFT, we simply changed the off-centered DFT to a centered DFT. After replacing **F** with its centered version we got another matrix **B** which commutes with centered DFT. i.e. $[\mathbf{B}, \mathbf{W}] = \mathbf{B}*\mathbf{W} - \mathbf{W}*\mathbf{B} = 0$, where **W** is a centered DFT.

2.3 The Infinite Order Second Derivative Approximation Method

Inspired by the work of Grunbaum [7], Pei, Hsue and Ding proposed another DFT-commuting matrix in [1], whose eigenvectors are even closer to the continuous G-H function than those of the Dickinson-Steiglitz matrix. The matrix proposed by them is given as;

$$\mathbf{M}_{2k} = \sum_{m=1}^{k} (-1)^{m-1} \frac{2[(m-1)!]^2}{(2m)!} \mathbf{D}^m, \tag{6}$$

where

$$\mathbf{D} = \begin{bmatrix} -2 & 1 & 0 & \dots & \dots & 0 & 1 \\ 1 & -2 & 1 & \dots & \dots & 0 & 0 \\ 0 & 1 & -2 & \dots & \dots & \vdots & \vdots \\ \vdots & \vdots & \vdots & \ddots & \ddots & \vdots & \vdots \\ 1 & 0 & 0 & \dots & \dots & 1 & -2 \end{bmatrix} \sim \text{the second order symmetric difference matrix.} \tag{7}$$

For the purpose of this report, we have used $k = 2$. Therefore, for $k = 2$;

$$\mathbf{M}_4 = \frac{-1}{12}\mathbf{D}^2 + \mathbf{D}. \tag{8}$$

Now the DFT commuting matrix based on this analysis is proposed as;

$$\mathbf{S}_4 = \mathbf{M}_4 + \mathbf{W}\mathbf{M}_4\mathbf{W}^{-1}. \tag{9}$$

We referred to this matrix $\mathbf{S}_4$, which commutes with DFT, as a higher-order S-matrix for the purpose of this report. If we change the off-centered DFT to its centered version, then the higher-order S-matrix will become commutable with the centered DFT. We again plotted eigenvectors and eigenvalues to compare them with those of sampled continuous G-H functions.

2.4 The Grunbaum Method

Another approach to obtaining the DFT eigenvectors uses the tri-diagonal commuting matrix introduced by Grunbaum [7]. Mugler and Clary modified the Grunbaum tri-diagonal incorporating a scaling factor, and the resultant eigenvectors very closely resemble the G-H functions [8]. The tri-diagonal commutor of Grunbaum is defined via its diagonal and off-diagonal elements in [8] as;

$$\mathbf{T}_{mn} = \begin{cases} -2\cos(\pi N\tau)\sin(\pi\mu\tau)\sin(\pi(N-\mu-1)\tau), & \text{if m = n ,0} \leq \text{ n } \leq \text{ N-1} \\ \sin(\pi\mu\tau)\sin(\pi(N-\mu)\tau), & \text{if m = n + 1, n - 1,} \\ & 1 \leq \text{ n } \leq \text{ N-1} \\ 0, & \text{otherwise} \end{cases}, \tag{10}$$

where $0 \leq \mu \leq N-1$ and $\tau = \frac{1}{N}$.

Santhanam and Vargas-Rubio focused their attention on the centered version of the DFT matrix operator $\mathbf{W}$ [12].

$$\mathbf{W}_{mn} = \frac{1}{\sqrt{N}} e^{(-j\frac{2\pi}{N}(m-a)(n-a))}, \tag{11}$$

where the shift parameter $a = \frac{N-1}{2}$. The eigenvalues of the commuting matrix $\mathbf{T}$ for the centered DFT are both real and unique and furnish the complete orthogonal set of DFT eigenvectors.

2.5 Quantum Mechanics in Finite Dimensions (QMFD)

Santhanam et. al. defined a discrete version of the G-H differential operator $\mathbf{H}$ [3] that furnishes the basis for the centered version of the DFT matrix and simultaneously has eigenvalues and eigenvectors that very closely resemble those of the continuous G-H operator. They utilized concepts from quantum mechanics in finite dimensions and [3], in the context of the discrete harmonic oscillator to the basis. The CDFT commuting matrix they defined is given as;

$$\mathbf{T} = c_1(\mathbf{P}^2 + \mathbf{Q}^2) + c_2\mathbf{C}_1^H\mathbf{C}_1 + c_3\mathbf{I}, \tag{12}$$

where $c_1 = 1, c_2 = -c_3 = -\frac{\pi^2}{N^2}$, N is the size of DFT matrix,

$\mathbf{P} = \mathbf{W}\mathbf{Q}\mathbf{W}^H$,

$\mathbf{Q}_{rr} = q[r] = \sqrt{\frac{2\pi}{N}}r, \ -\frac{N-1}{2} \leq r \leq \frac{N-1}{2}$,

$\{\mathbf{W}\}_{mn} = \frac{1}{\sqrt{N}} e^{(-j\frac{2\pi}{N}(m-a)(n-a))}$ is a centered version of the DFT matrix ,

$a = \frac{N-1}{2}, \ 0 \leq m,n \leq (N-1)$,

$\mathbf{C}_1 = \mathbf{QP} - \mathbf{PQ}$ and

$\mathbf{I}$ is the identity matrix of dimension N.

We changed the range of r that normally spans $r \in \left[-\frac{N-1}{2}, \frac{N-1}{2}\right]$ to the zero locations of the Nth order G-H function to see improvement in terms of linearity of the eigenvalues and the invertibility region in the peak-to-parameter mapping, and we found slight improvement in both the parameters. Therefore, we retain the values

of r as the zero location of the N^{th} order G-H operator throughout the report, and we referred to this method as *'modified QMFD'* or 'QMOD'.

3 Multi-angle CDFRFT

Vargas-Rubio and Santhanam [11] discussed the multi-angle CDFRFT as;

$$\{\mathbf{A}_\alpha\}_{kn} = \sum_{p=0}^{N-1} v_{kp} v_{np} e^{-jp\alpha}, \tag{13}$$

where v_{kp} is the kth element of the pth eigenvector. Multiplying $\mathbf{A}_\alpha$ by the signal x[n], we obtain;

$$\mathbf{X}_\alpha[k] = \sum_{n=0}^{N-1} x[n] \sum_{p=0}^{N-1} v_{kp} v_{np} e^{-jp\alpha}. \tag{14}$$

For discrete set of angles $\alpha = \alpha_r = \frac{2\pi r}{N}$, $r = 0, 1, ..., N-1$

$$\mathbf{X}_k[r] = \sum_{p=0}^{N-1} z_k[p] \mathbf{W}_N^{pr}, \tag{15}$$

where

$$z_k[p] = v_{kp} \sum_{n=0}^{N-1} x[n] v_{np}. \tag{16}$$

Expressing the transform as a DFT allows us to use a radix-2 FFT algorithm to compute the CDFRFT. The resulting transform $\mathbf{X}_k[r]$ containing the CDFRFT for these discrete angles is called multi-angle DFRFT (MA-CDFRFT).

It is important to observe that $\mathbf{X}_k[0]$ corresponds to the original signal x[n] with k = n, and $\mathbf{X}_k[\frac{N}{4}]$ corresponds to the CDFT of x[n] when N is a multiple four, since in this case, $\alpha_{\frac{N}{4}} = \frac{\pi}{2}$. Figure 1 shows a graphical representation of the array $\mathbf{X}_k[r]$ to illustrate how index k has different interpretations depending on the value of r. For example, when r = 0, k is interpreted as time and when $r = \frac{N}{4}$, k corresponds to frequency. This interpretation also shows that the upper half of $\mathbf{X}_k[r]$ is a reversed version of the lower half.

We considered a chirp signal to discuss the above mentioned parameters as;

$$x[n] = e^{j(c_r m^2 + w_c n)},\ 0 \le n \le (N-1),\ m = n - \frac{N-1}{2}, \tag{17}$$

where, c_r = chirp rate and w_c = central frequency. We assumed $c_r = 0.001$ and $w_c = 0$ for this analysis.

We used the MA-CDFRFT approach to see where the peak occurs for a given chirp rate and a central frequency. Then we took a row (where the peak occurs) of the MA-CDFRFT matrix to plot the peak that corresponds to the given chirp rate and the central frequency. Figure 2 describes the magnitude of the MA-CDFRFT of the above signal obtained from five different methods. From this plot, we can observe that we actually have two maxima because the CDFRFT at $\alpha + \pi$ is the reversed version of the CDFRFT at α.

We can observe from figure 2 that the least fringe occurs with the Grunbaum basis and the QMOD method, which means that the Grunbaum method results in the least side-lobes for MA-CDFRFT in comparison to the other four methods, whereas the bilinear transformation method, the higher order S-matrix method and the D-S method produce larger sidelobes. We can see on a 2D plot of MA-CDFRFT that the two peaks on the magnitude plot of MA-CDFRFT occur at r = 68 and r = 196 for all the methods. We used only the lower half for our consideration. Then we took a slice of the MA-CDFRFT at r = 68. Figure 3 shows the slice of the MA-CDFRFT at r = 68 for all the methods.

From figure 3, it is clear that the sharpest peak is obtained with the QMOD method. . Hence we can conclude that the QMOD method is the best among the five methods in terms of sharpness of the peak obtained from the MA-CDFRFT approach.

4 Results

4.1 Performance Metrics

While each of the methods produce a peak in the chirp rate versus frequency plane for a chirp signal, the sharpness and the width of the peak varies based on the basis used. In this section, we attempt to quantiy this ability by comparing the methods with respect to following metrices. In the ideal case, a chirp would be transformed into a Dirac impulse for a specified center frequency and chirp rate.

4.1.1 Mainlobe-to-Sidelobe Ratio

In antenna theory, main-lobe is the lobe containing the maximum power whereas side-lobes are the lobes that are not the main lobe, and the ratio of the power of these two lobes is defined as mainlobe-to-sidelobe ratio. For the purpose of this report, in the same fashion, the ratio of the peak value to the value of the second peak is defined as the mainlobe-to-sidelobe ratio. We can see those peak values and side-lobes in figure 3. In order to compute mainlobe-to-sidelobe ratio we first took the absolute value of the row of MA-CDFRFT matrix where the peak occurs. We then consider the highest peak as mainlobe and the second peak as sidelobe. Finally, we took the ratio of these two values as mainlobe-to sidelobe ratio (MLSLR). Figure 4 shows the mainlobe-to-sidelobe ratio for different combinations of c_r and w_c.

From these figures, it is clear that the MLSLR increases as N increases only in the case of the Grunbaum basis. Also, the QMOD method has a better MLSLR in the case of zero central frequency until N = 512, whereas the Grunbaum method has a better MLSLR in the case of non-zero central frequency. Therefore, we can conclude that the QMOD method and the Grunbaum method are the best choice among the five methods towards attaining a better MLSLR. We observed that the MLSLR decreases for some methods for higher values of N. This is due to the fact that the MA-CDFRFT approach picks more side lobes as we increase transform size.

4.1.2 10-dB Bandwidth

In communication systems, the X-dB bandwidth of a communication channel is the part of the system's frequency response that lies within X-dB of the response at its peak, which in the pass-band filter case is typically at or near its center frequency, and in the lowpass filter is near 0 hertz. If the maximum gain is 0 dB, the X dB gain is the range where the gain is more than -X dB, or the attenuation is less than X dB. Similarly, 10-dB bandwidth, in this thesis, is defined as the range of frequencies where the signal[1] has its value 10 dB below the peak value of the signal. Figure 5 shows the 10-dB bandwidth comparison for different combinations of c_r and w_c. From these figures, we can see that the bandwidth continuously decreases only for the QMOD basis in the case of zero central frequency. And for non-zero central frequency, the bandwidth continuously decreases as N increases. The bilinear transformation method and the S-matrix method have the least bandwidth for non-zero central frequency.

4.1.3 Quality Factor

Quality factor, also known as Q-factor, is a dimensionless quantity which characterizes a signal's bandwidth relative to its central frequency. It measures the quality of the peak in relationship with central frequency. Math-

[1] Signal refers to the magnitude of a slice of the MA-CDFRFT matrix at r = 36.

ematically, it is the ratio of the central frequency to the bandwidth of the signal. i.e.

$$Q - factor = \frac{w_c}{BW}, \tag{18}$$

where w_c = Central frequency and BW = Bandwidth of the signal.

We set the central frequency as $\frac{\pi}{4}$ and chirp rate as 0.0005 in equation (17) to find the Q-factor of the peaks for all the five methods. Therefore the signal used to find Q-factor became;

$$x[n] = e^{j(0.0005m^2 + \frac{\pi}{4}n)}, \;\; 0 \leq n \leq 255, \; m = n - \frac{255}{2}. \tag{19}$$

Figure 6 depicts the Q-factor comparison for $c_r = 0.0005$ and $w_c = \frac{\pi}{4}$. From this plot, it is clear that the Q-factor increases for all the bases as N increases, which is obvious from the previous section, because the lower bandwidth requirement for a fixed center frequency is equivalent to a higher quality factor. We can see from the figure that the bilinear transformation method and the S-matrix method are the best choice in terms of Q-factor considerations.

4.1.4 Linearity of the Eigenvalues Spectrum

Santhanam et. al. in [6] stated that eigenvalues of the G-H opertor are linearly spaced. Therefore the eigenvalues of the matrices obtained from all the five different approaches, should be linear in spacing in order to resemble the eigenvalues of the continuous G-H operator. We first plotted the eigenvalues of the five different matrices, as shown in figure 7, to determine the extent of the linearity of eigenvalue spectrum. Then we calculated the percentage of number of points where the eigenvalues spread linearly for different values of N. Figure 8 shows the percentage of number of points where the eigenvalues are as linear as that of the continuous G-H operator.

From figure 8, it is evident that the eigenvalue spectrum from the QMOD method best resembles those of the continuous G-H operator. They are linear for about 80% of the total points which is far better than all other methods. Furthermore, this linearity steadily increases with increase in N, a fact consistent with the assymptotic convergence of the QMFD matrix to the continuous G-H operator. The linearity of the eigenvalue spectrum is directly related to the invertible region for the peak-to-parameter mapping which we will discuss in a later section of this report.

4.1.5 Error-norm of the Eigenvectors

The eigenvectors of the matrices obtaoined from the five different approaches look like the corresponding G-H function; however they are not exactly the same. Pei, Hsue and Ding defined the error-norm of eigenvectors as the second norm of the difference between the eigenvectors obtained from the G-H like eigenvector[2] and the samples of its corresponding continuous G-H function [1]. We, therefore, plotted the error-norm of the eigenvectors for all the five different methods for N = 64 to determine eigenvectors of which matrix better resembled those of the sampled continuous G-H operator. Figure 9 depicts the error-norm comparison for N = 64 for all the methods we discussed.

From this figure, it is clear that the error-norm increases as the number of zero crossings increases for all the methods, as we discussed in the previous chapter. We can also see that the QMOD method results in a very low error-norm in comparison to the other four methods. Therefore, eigenvectors of the QMOD matrix better resemble the eigenvectors of the corresponding G-H operator in comparison to the other four methods.

[2] G-H like eigenvectors are the eigenvectors of any of the matrices that commute with the DFT.

4.1.6 Chirp Parameter Estimation Error

Subspace decomposition techniques have been investigated for use in conjunction with the DFRFT with the aim of providing a robust and accurate estimation in the presence of noise [9]. Peacock and Santhanam discussed the chirp parameter estimation error using 2D peak picking [4]. We used parameter estimaion error as one of the bases for comparison of five proposed approaches. We measured the parameter estimation error of those five approaches and compared them to the Cramer-Rao lower bound and resolution bound. Figure 10 shows the parameter estimation error using 2D peak picking for central frequency and chirp rate, for N = 256.

From this figure, we can see that the estimation error for the QMOD method attains the resolution bound for higher SNR for both center frequency estimation and chirp rate estimation, and the error for the Grunbaum method is close to that of the QMOD method. However the other three methods result in significantly more parameter estimation errors. This is because the peak-to-parameter mapping depicts multiple disconnected regions of chirp parameters mapping to the same peak location. We can also see that, both the center frequency estimation and chirp rate estimation for the bilinear transformation method do not decrease as gradually as in other methods. This is because of the fact that the particular combination of center frequency and chirp rate, where the mean square error goes up, does not lie withn the invertible mapping region. Figure 11 shows the parameter estimation error calculated using the cross-hair technique combined with the minimum-norm-subspace technique. From this figure, we can see that the chirp parameter estimaion error for the QMOD method approaches the Cramer-Rao lower bound for chirp parameter estimation [10]. From this analysis, we can conclude that either of these techniques has more success using the QMOD basis.

4.1.7 Peak-to-Parameter Mapping Region

Application of the DFRFT to chirp parameter estimation is not meaningful if a complete analysis of the invertibility of mapping is ignored. Therefore we looked at the peak-to-parameter mapping region in the $\alpha - \omega$ plane to see where the mappings satisfied the connectivity and adjacency conditions. The connectivity criteria is satisfied when the set of all chirp parameters that map to a single location in the chirp-rate versus center-frequency plane form a connected set, and adjacency criteria is satisfied when locations which are adjacent in the transform plane map to adjacent regions in the chirp parameter space. We calculated the mapping regions where both connecticity and adjacency criteria were satisfied for all the five methods. We calculated the percentage of pixels in which both the connectivity and adjacency conditions were satisfied. Upon doing this, we had a clear idea of which method, among the five proposed methods, had the best valid mapping region in comparison to the expected mapping region shown in figure 12. Figure 13 depicts the percentage of pixels in $\alpha - \omega$ plane where both connectivity and adjacency criteria are fulfilled.

From these mapping regions, we can see that the connectivity and adjacency conditions are not fulfilled for large regions in the case of the bilinear transformation method, the S-matrix method and the higher order S-matrix method. The regions in which these two conditions are violated overlap in these three cases. In the case of Grunbaum method, we can see that, the two conditions are not satisfied in two different regions. The connectivity criteria is almost satisfied in the diamond region for the Grunbaum method, but the adjacency criteria is not satisfied as expected in the diamond region. Finally, both the criteria are satisfied in almost entire region of the $\alpha - \omega$ plane for the case of the QMOD method.

From this comparison, we can also see that the QMOD technique is the only method in which the percentage of mapping pixels satisfying both the connectivity and adjacency criteria, increases as N increases. This fact is further related to the linearity of the eigenvalue spectrum. We saw in section 4.1.4 that the linearity of the eigenvalue spectrum increases when N increases only in the case of the QMOD basis. We also observed that the percentage of eigenvalue linearity for the QMOD method is far above than that of all other methods. From figure 13, we can see that the percentage of pixels reaches almost 90% for the QMOD method for N = 512, which is far better than all the other methods. This confirms the fact that the QMOD basis produces the least estimation error because it has the largest valid peak-to-parameter mapping region in the $\alpha - \omega$ plane. We can also say that the valid mapping region will cover the entire $\alpha - \omega$ plane if N is sufficiently large for the QMOD basis. Note that if

the valid mapping region spreads over the entire $\alpha - \omega$ plane, it will correspond to the case in which there is no estimation error for both center frequency and chirp rate.

4.2 The Joint Diagonalization Method

All the methods that we have discussed so far are unable to produce eigenvalue spectrum that is strictly linear. Similarly, none of these approaches produces a valid mapping region for the entire $\alpha - \omega$ plane. We therefore combined the two approaches- the Grunbaum method and the QMOD method- to see whether this combination would produce more linearity in eigenvalues than that of either of the methods. Our intention in using joint diagonalization was also to get a better valid mapping region than that of the individual methods. This joint diagonalization can be obtained using the matlab function 'eig'.

$$[V,D] = eig(T_g, T_Q), \tag{20}$$

where V = eigenvectors, D = digonalized eigenvalues, T_g = CDFT matrix obtained using the Grunbaum method and T_Q = CDFT matrix obtained using the QMOD method. The eigenvalues obtained from this joint diagonalization are depicted in figure 14. We then calculated the linearity of the eigenvalue spectrum obtained using the joint method, but we did not observe any improvement in linearity. In fact, the linearity decreased in comparison to the QMOD method.

We also checked the valid mapping region corresponding to the joint method. Figure 15 depicts the valid mapping region for the joint diagonalization method. Contrary to our expectation , we did not observe any improvement in the mapping region in terms of invertibility area. From these observations, we can conclude that the joint diagonalization method would not produce any improvement in the linearity of eigenvalue spectrum and in the inverbility mapping region in comparison to the individual methods. In fact, the joint method produces the average of the results of the two methods used in joint diagonalization.

4.3 Relation between α and c_r

For better concentration of signal energy when analyzing linear chirps, an α between 45° to 135° is a good choice [11]. For this interval, an empirically developed relationship between the angle of transform and chirp rate, with corresponding error less than 2%, is given as;

$$c_r = 2\frac{\tan\left(\alpha - \frac{\pi}{2}\right)}{N} + 1.41\frac{\left(\alpha - \frac{\pi}{2}\right)}{N}, \tag{21}$$

with $\alpha = \frac{2\pi r}{N}$.

This relationship is useful in determining the chirp rate from the angle, particularly when we use the MA-CDFRFT algorithm.

We determine the chirp rate using equation (21) for the signal in equation (17) with $c_r = 0.001$, where we found that the peak occurs at r = 69 for N = 256,

$$\alpha = \frac{2\pi r}{N} = 1.6935,$$

and c_r = 0.00163. This is close to 0.001, which is the value we took in this particular case. Table I shows the chirp rate obtained using equation (21). From this table we can see that the chirp rate obtained from the equation is very close to the actual chirp rate. This confirms that equation (21) may be used to estimate the chirp rate to a resonable accuracy.

Peacock and Santhanam [4] have derived an expression for the peak-to-parameter mapping. Using this expression for the QMOD method, they produce a mapping region which is very similar to the continuous mapping for $\omega < \frac{\pi}{3}$,

$$c_r = -\frac{\pi}{N}\cot\left(\frac{k\pi}{N}\right) \qquad and \qquad \omega = \frac{2\pi}{N}\left(r - \frac{N-1}{2}\right)\csc\left(\frac{k\pi}{N}\right), \tag{22}$$

Actual Chirp Rate	Chirp Rate using Equation 21
-0.012176346	-0.011628762
-0.008356316	-0.008056398
-0.004536286	-0.004338268
-0.000716256	-0.000326968
0.003103774	0.003649013
0.006923804	0.007656638
0.010743834	0.010743834

Table I: Comparison between actual chirp rate and the chirp rate obtained from equation (21)

Actual Parameters		Parameters obtained from equation 23	
ω_c	C_r	$\hat{\omega}_c$	$\hat{C}_r$
$\frac{\pi}{4}$	0.001	0.8015	0.0012
$\frac{\pi}{4}$	0.002	0.7846	0.0021
$\frac{\pi}{4}$	0.003	0.7970	0.003
$\frac{\pi}{4}$	0.004	0.7883	0.004
$\frac{\pi}{4}$	0.005	0.7836	0.005
$\frac{\pi}{4}$	0.006	0.7831	0.0061

Table II: Comparison of actual chirp rates and chirp rate estimates from equation (23)

where c_r is chirp rate and ω is central frequency

But we found that this mapping does not correcly map the peak location to the corresponding chirp rate and central frequency.

We then modified this peak to parameter mapping expression to correctly map the peak location to the corresponding chirp rate and central frequency as

$$\hat{C}_r = -\frac{\pi}{N}\cot\left(\frac{2r_p\pi}{N}\right) \qquad \textit{and} \qquad \hat{\omega}_c = \frac{2\pi}{N}\left(k_p - \frac{N-1}{2}\right)\csc\left(\frac{2r_p\pi}{N}\right), \tag{23}$$

where $\hat{C}_r$ is the estimatated chirp rate, $\hat{\omega}_c$ is the estimated central frequency, r_p is the coefficient index of peak location and k_p is the angular index of peak location.

Using this expression, we can obtain the peak-to-parameter mapping with average error of 0.4% for the QMOD method. Therefore we can conclude that equation (23) produces less error in terms of parameter estimation and peak to parameter mapping in comparison to equation (21). Table II depicts the example of the peak to pameter mapping for the QMOD method with G-H separation using equation (23).

5 Conclusions

In this report, we studied the centered DFRFT, its properties, the nature of its eigenvalues and eigenvectors, and its relationship with linear chirp signals. The main objective of this research was to find the best algorithm to use for the computation of the centered version of DFRFT. We studied some properties of each of the CDFRFT matrices that were obtained from the different approaches. We looked at the eigenvalues and eigenvectors of those matrices to see whether or not they resembled those of the continuous G-H operator. We also calculated the error-norm of eigenvectors to determine whether or not there were any deviations of those eigenvectors from those of the corresponding G-H function. In addition, we calculated the chirp parameter estimation errors using 2D peak detection in the MA-CDFRFT chirp-rate versus central-frequency plane. Finally, we measured the peak-to-parameter mapping regions where connectivity and adjacency criteria were satisfied. The main findings of this research can be summarized as follows.

Among all the five methods discussed in this thesis, the QMOD method, a method in which the diagonal matrix **Q** takes its diagonal as the zero crossings of the Nth order G-H function instead of taking its diagonal as equally spaced values in between $-\frac{N-1}{2}$ and $\frac{N-1}{2}$ used in the conventional QMFD method, produces the sharpest peak for single chirp application. This result was verified by using different metrics such as mainlobe-to-sidelobe ratio, 10-dB bandwidth, and quality factor. Also, the QMOD method produces the best linearity on eigenvalues, which confirms the fact that the eigenvalues obtained from the QMOD method are closest to the eigenvalues of the continuous G-H operator. The same method results in less error-norm than the other methods, which confirms that the eigenvectors of the QMOD matrix are closest to that of sampled continuous G-H operator.

As is evident from the previous section, the QMOD method produces the least parameter estimation error for both center frequency estimation and chirp rate estimation. This estimation error almost attains the Camer-Rao lower bound when it is calculated for the QMOD method in combination with the cross-hair estimation technique. As we saw in the previous chapter, the QMOD method has an invertibility region of almost 90% of the $\alpha - \omega$ plane, which is far better than those of the other four methods. Therefore, we can conclude from our study that the deviation from a fully linear eigenvalue spectrum of the DFT commuting matrix produces a large proportion of peak-to-parameter mapping pixels where the invertibility criteria are violated, and loss of invertibility results in larger chirp parameter estimation error.

References

[1] S.C. Pei, W.L. Hsue and J.J. Ding, DFT-Commuting Matrix With Arbitrary Or Infinite Order Second Derivative Approximation, *IEEE Transactions on Signal Processing*, Vol. 51, No. 1, (January 2009)

[2] A. Serbes and L. Dural-Ata, Eigenvectors Of The Discrete Fourier Transform Based On The Bilinear Transform, *Eurasip Journal on Advances in Signal Processing*, Vol. 2010 Article ID. 191085

[3] B. Santhanam and T.S. Santhanam, On discrete Gauss-Hermite Functions And Eigenvectors Of The Discrete Fourier Transform, *Signal Processing, Elsevier Science*, Vol. 88, No. 6, Pages 2738 - 2746, (November 2008)

[4] D.J. Peacock and B. Santhanam, Comparison Of Centered Discrete Fractional Fourier Transform For Chirp Parameter Estimation, *Proc. of IEEE DSP/SPED Workshop*, (August 2013)

[5] B.W. Dickinson and K. Steiglitz, Eigenvectors And Functions Of The Discrete Fourier Transform, *IEEE Transactions on Acoustics, Speech and Signal Processing*, Vol. 30, No. 1, (February 1982)

[6] B. Santhanam and T.S. Santhanam, Discrete Gauss Hermite Functions And Eigenvectors Of The Centered Discrete Fourier Transform, *Proc. of ICASSP 2007, Honolulu*, Pages 418 - 422, (April 2007)

[7] F.A. Grunbaum, The Eigenvectors Of The Discrete Fourier Transform: A Version Of The Hermite Functions, *Journal of Mathematical Analysis and Applications*, Vol. 88, Pages 355 - 363, (1982)

[8] S. Clary and D.H. Mugler, Shifted Fourier Matrices And Their Tri-Diagonal Commutors, *SIAM Journal Matrix Analysis & Applications*, Vol. 24, No. 3, Pages 809 - 821, (2003)

[9] B. Santhanam and M. Hayat, On A Pseudo-Subspace Framework For Discrete Fractional Fourier Transform Based Chirp Parameter Estimation, *Processing of IEEE DSP/SPE Workshops*, Pages 360 - 363, (2011)

[10] D.J. Peacock and B. Santhanam, Multicomponent Subspace Chirp Parameter Estimation Using Discrete Fractional Fourier Analysis, *Processing of IASTED Conference on SIP-2011*, Pages 326 - 333, (December 2011)

[11] J.G. Vargas-Rubio and B. Santhanam, The Centered Discrete Fractional Fourier Transform And Linear Chirp Signals, *Proc. of 11th IEEE DSP & DSP Education Workshop, Taos Ski Valley, New Mexico*, Pages 163 - 167, (August 2004)

[12] B. Santhanam and J.G. Vargas-Rubio, On the Grunbaum Commuter Based Discrete Fractional Fourier Transform, *Proc. of ICASSP-04, Montreal, Canada*, Vol. II, Pages 641 - 644, (May 2004)

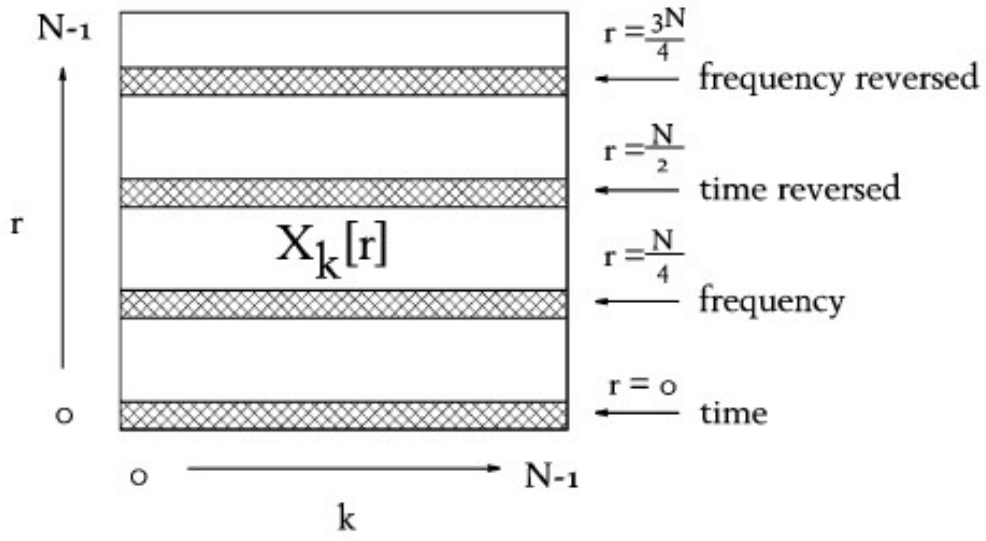

Figure 1: Graphical representation of $\mathbf{X}_k[r]$ that shows how the interpretation of the index k changes depending on the value of index r.

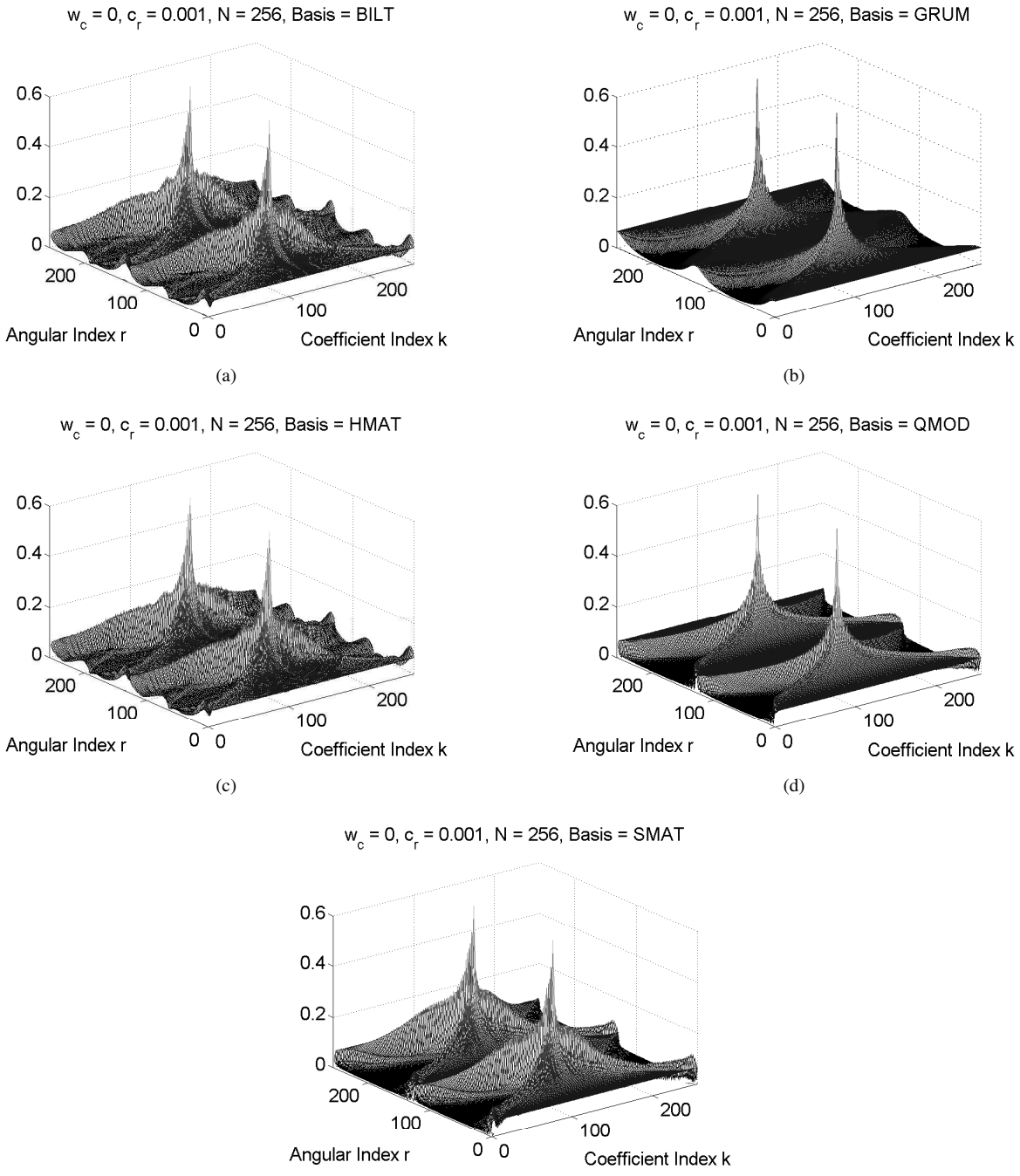

Figure 2: 3D plot of magnitude of MA-CDFRFT at $c_r = 0.001$ and $w_c = 0$ for N = 256 obtained from (a) Bilinear transformation method, (b) Grunbaum method, (c) Higher order S-matrix method, (d) QMOD method and (e) S-matrix method. The QMOD method produces the sharpest peak with least sidelobes.

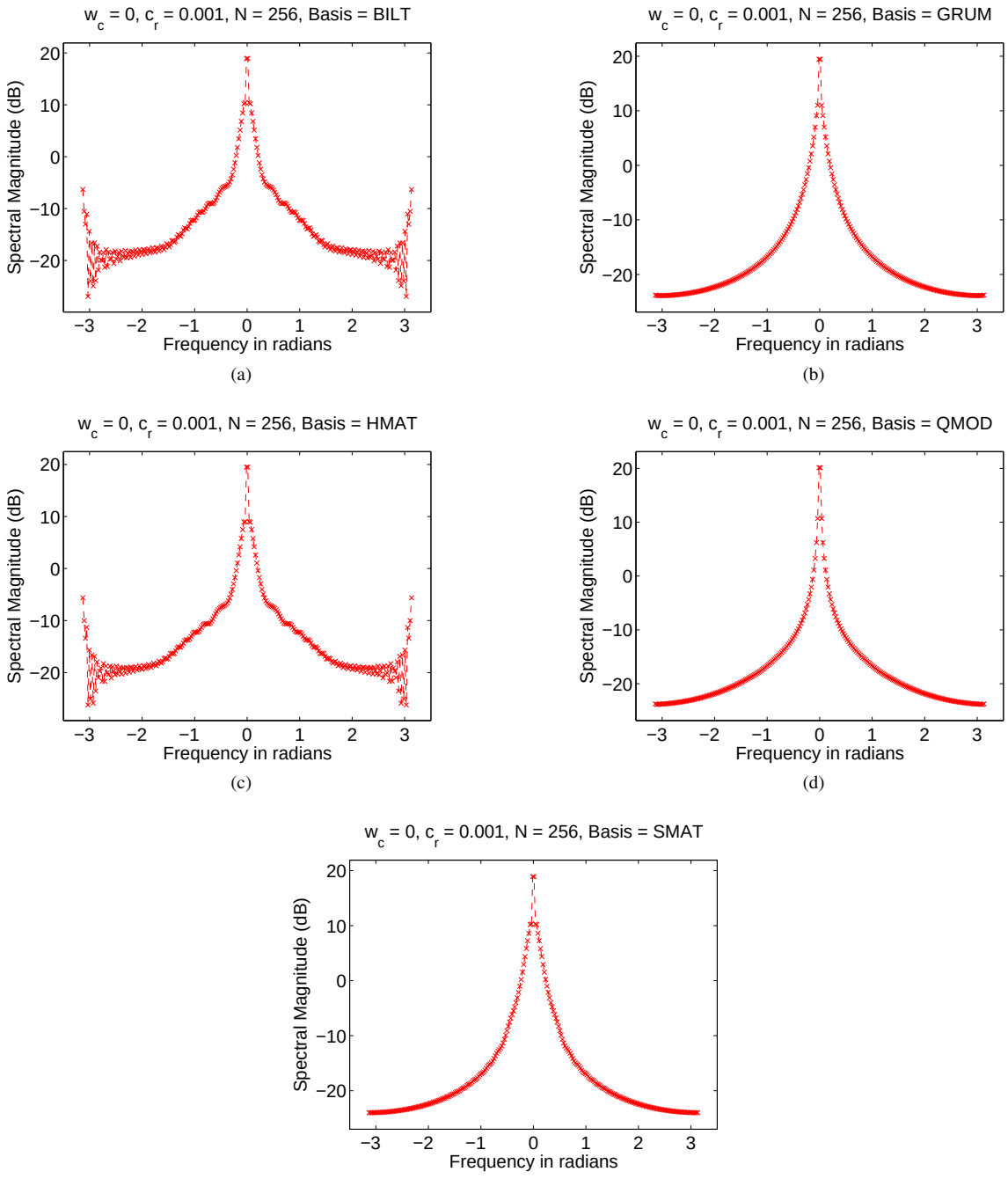

Figure 3: Plot of slice of MA-CDFRFT at r = 68 for $c_r = 0.001$, $w_c = 0$ and N = 256 obtained from (a) Bilinear transformation method, (b) Grunbaum method, (c) Higher order S-matrix method, (d) QMOD method and (e) S-matrix method. The QMOD method produces the sharpest peak with least sidelobes.

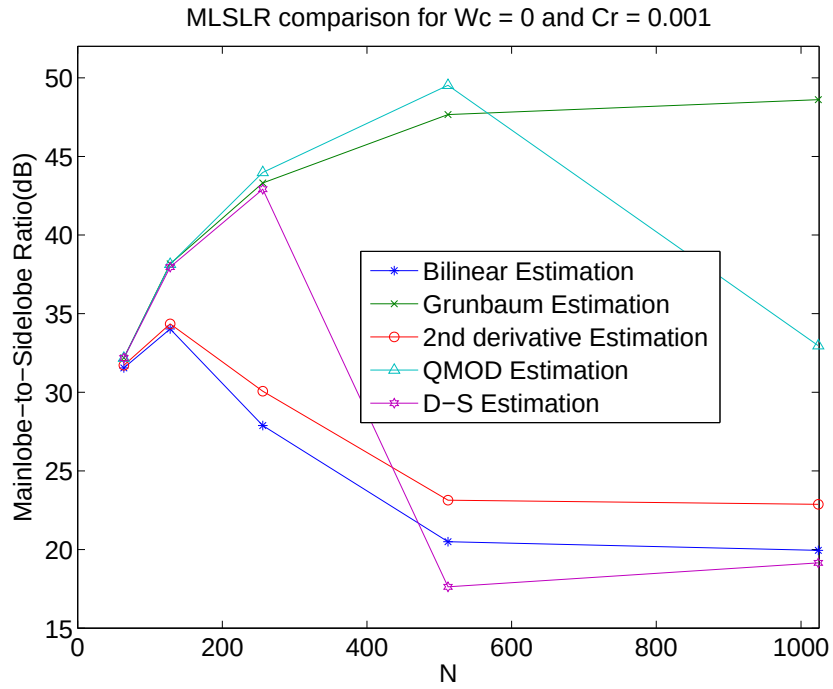

(a)

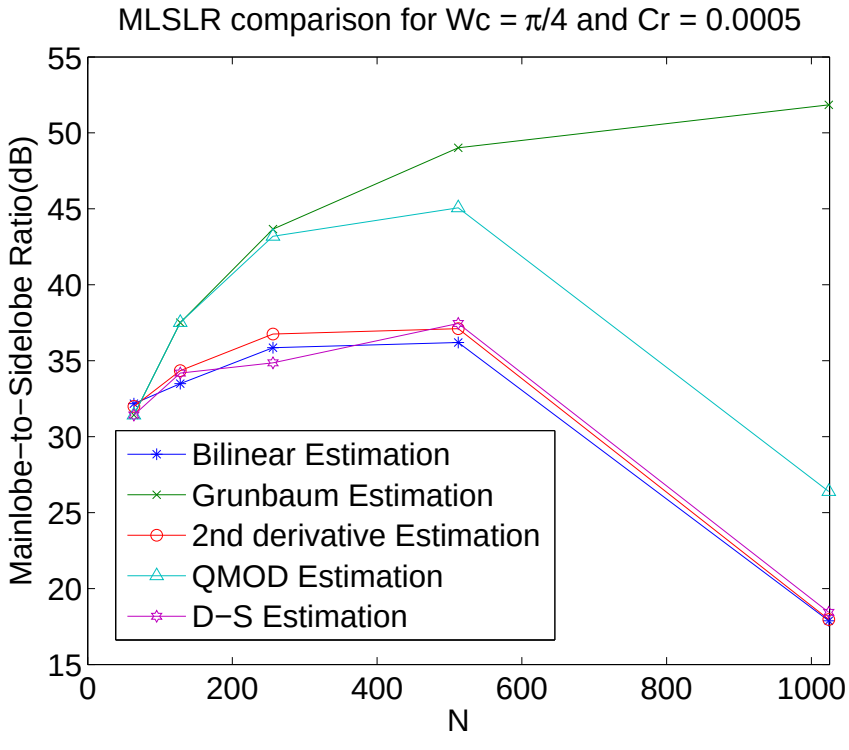

(b)

Figure 4: Mainlobe-to-Sidelobe ratio comparison of a peak obtained for a chirp with (a) $c_r = 0.001$ and $w_c = 0$ and (b) $c_r = 0.0005$ and $w_c = \frac{\pi}{4}$. Grunbaum method exhibits a steady increase in MLSLR.

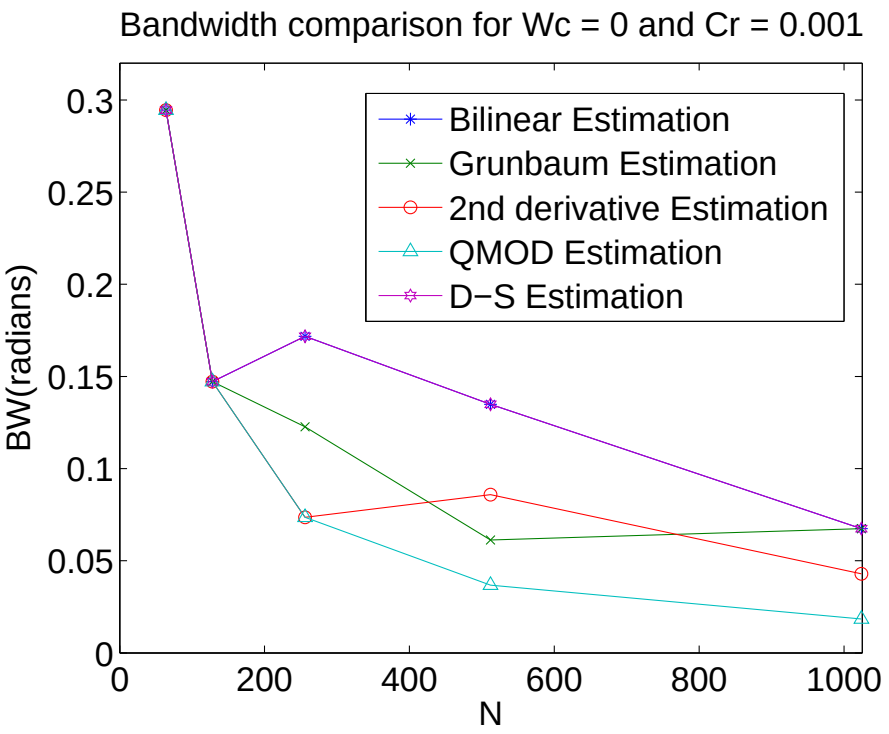

(a)

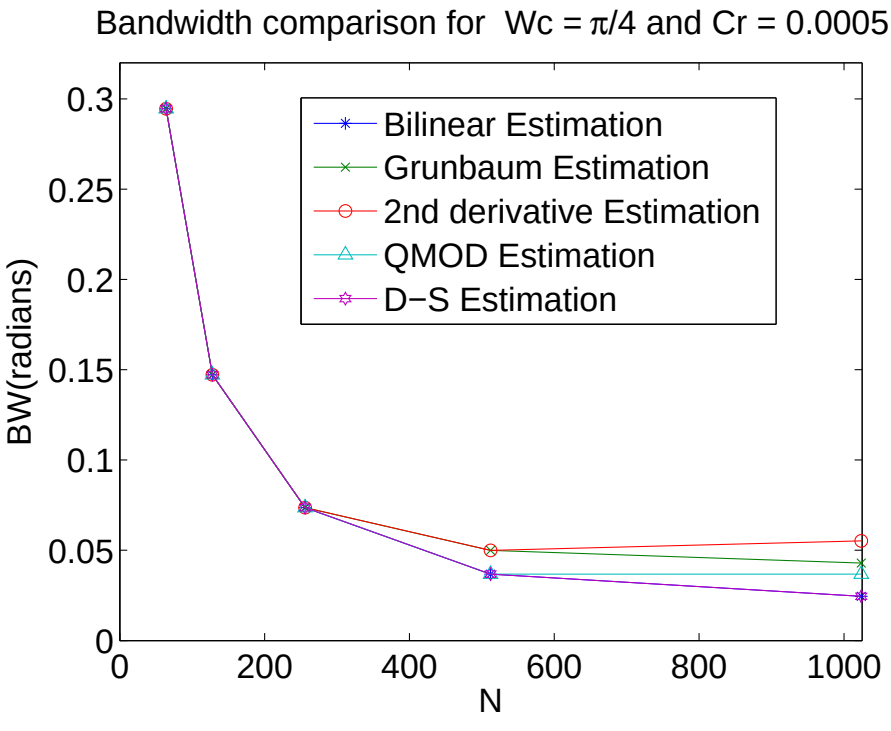

(b)

Figure 5: 10-dB BW comparison for (a) $c_r = 0.001$ and $w_c = 0$ and (b) $c_r = 0.0005$ and $w_c = \frac{\pi}{4}$. QMOD method exhibits a steady decrease in BW with increase in N for a chirp signal with zero central frequency. For non-zero central frequency, all the five methods exhibit a steady decrease in BW with increase in N, but the S-matrix method and the bilinear trasnformation method produce best result in terms of BW.

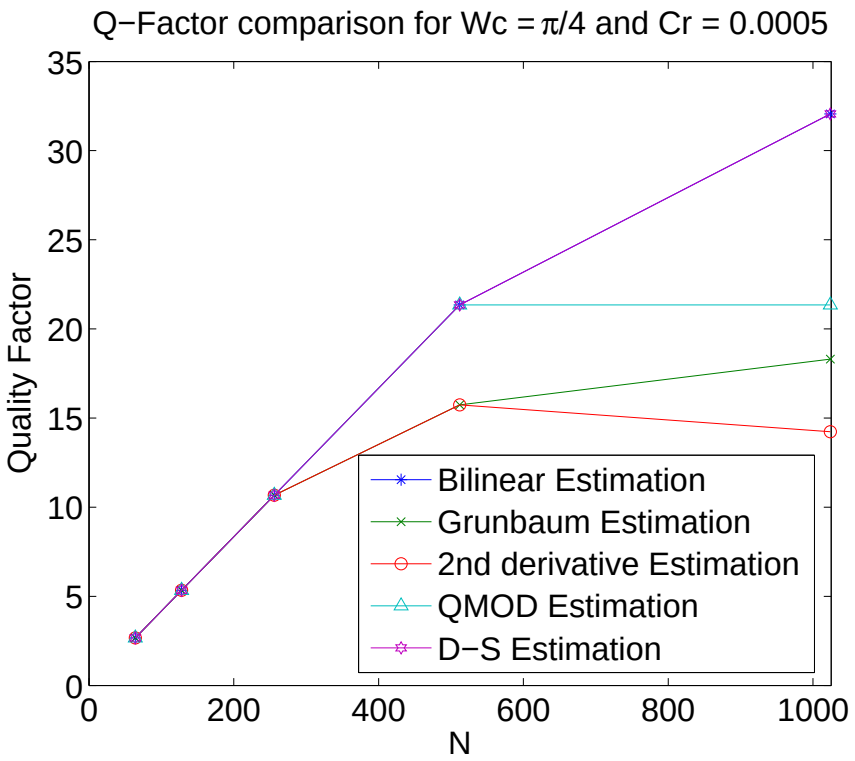

Figure 6: Q-factor comparison of peak obtained for a chirp with $c_r = 0.0005$ and $w_c = \frac{\pi}{4}$. The S-matrix method and the bilinear trasnformation method produce best result in terms of Q-factor. This obvious because the lower BW requirement for a fixed center frequency is equivalent to a higher Q-factor.

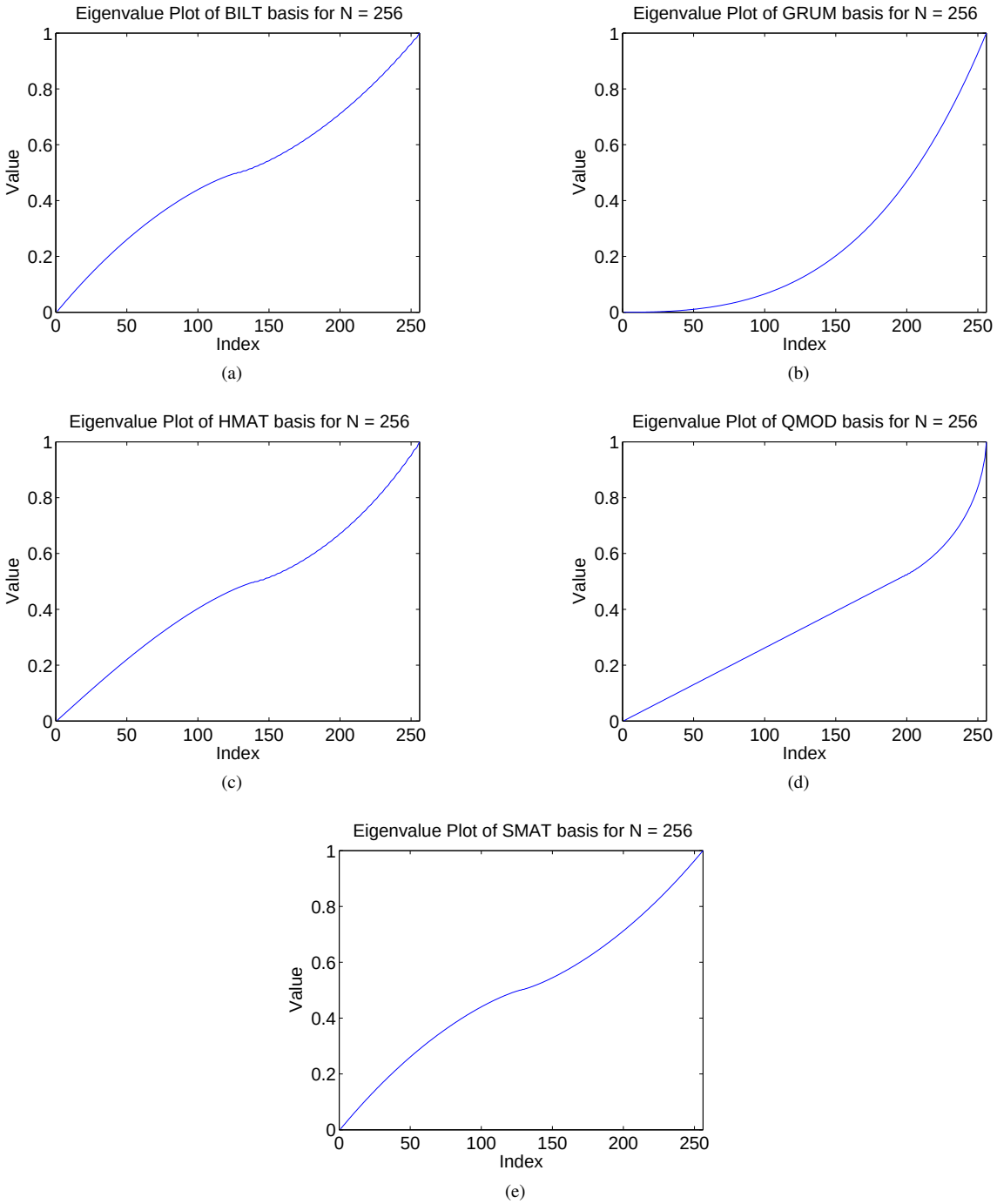

Figure 7: Eigenvalue spectrum for N = 256 obtained from (a) Bilinear transformation method, (b) Grunbaum method, (c) Higher order S-matrix method, (d) QMOD method and (e) S-matrix method. The QMOD method produces the most linear eigenvalue spectrum.

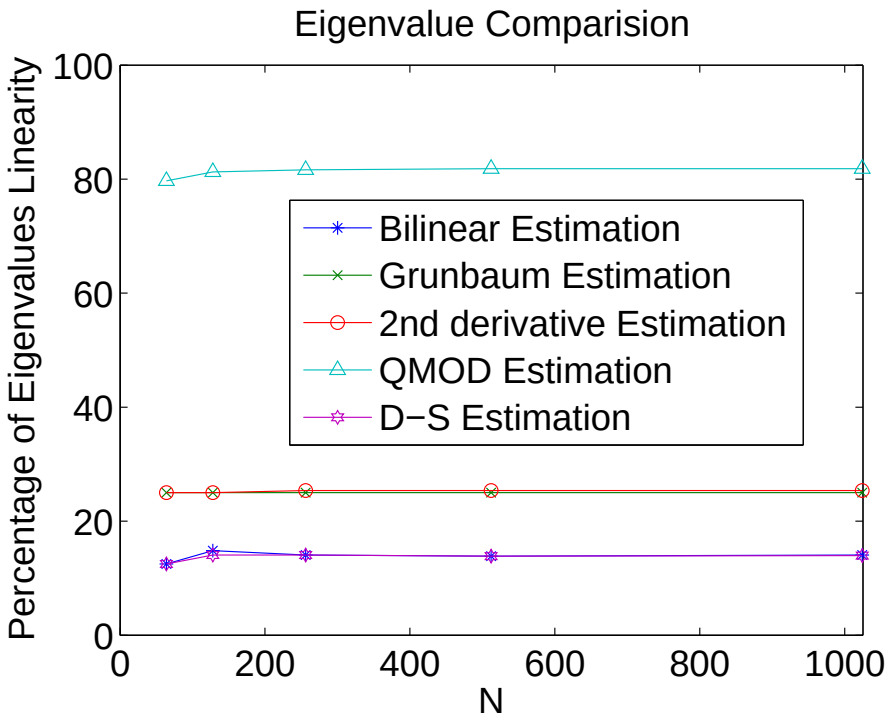

Figure 8: Percentage of number of points where eigenvalue spacing is linear. The QMOD method exhibits a far better linearity of eigenvalues spectrum. This means the eigenvalues of QMOD matrix are closest to those of continuous G-H operator.

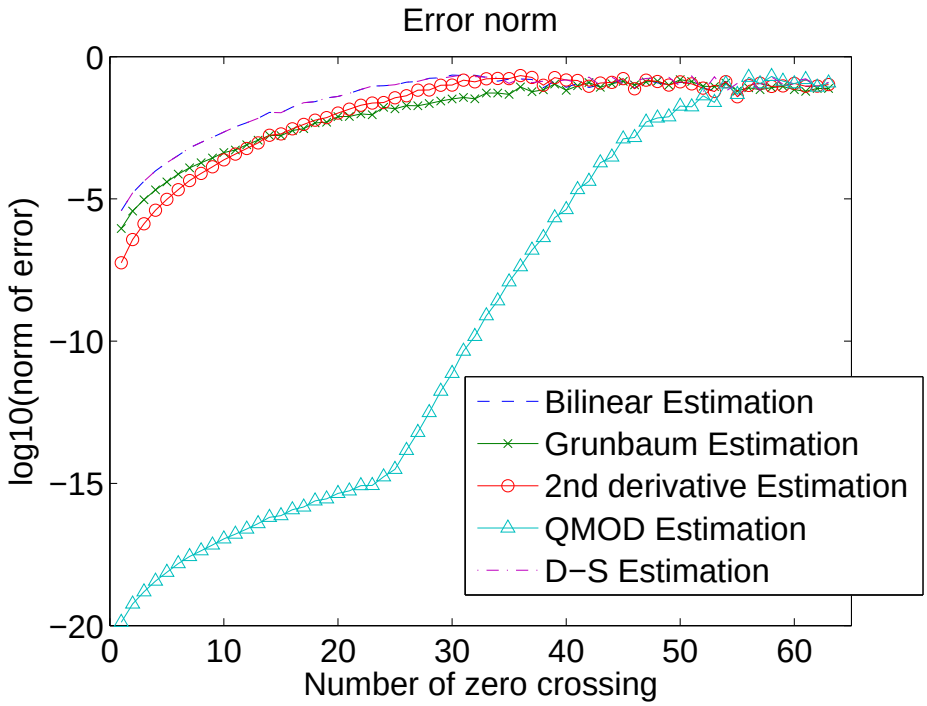

Figure 9: Error-norm comparison for N = 64. The QMOD method exhibits the least error norm for smaller values of zero-crossings. This means the eigenvectors of the QMOD matrix are closest to those of the sampled continuous G-H operator.

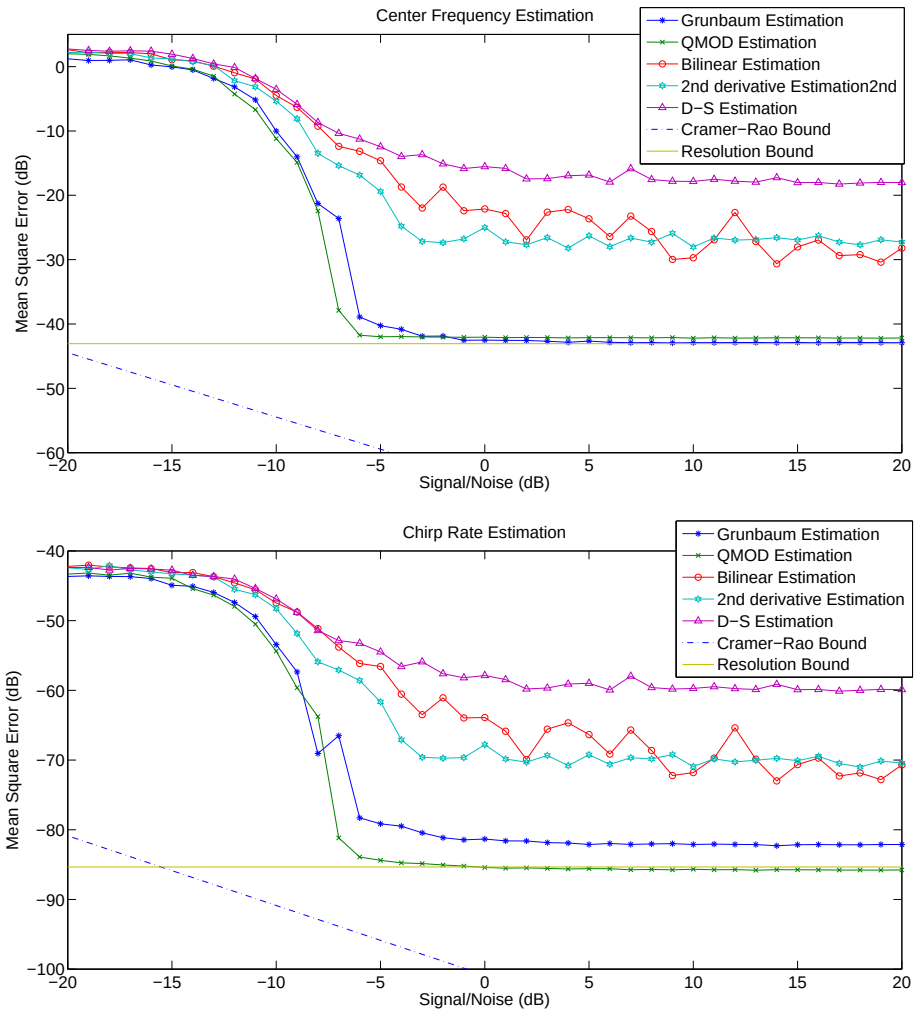

Figure 10: 2D parameter estimation error: The MSE was calculated at each SNR using 1000 chirps of length N = 256, in the 'safe' range of $|\alpha|(N-1)+|w| = IF < 0.85\pi$. A transform of size *NXN* was used, refined using minimum norm subspace decomposition and FFT of size R = 4096. Note that the QMOD method produces the least mean square error for both center frequency estimation and chirp rate estimation.

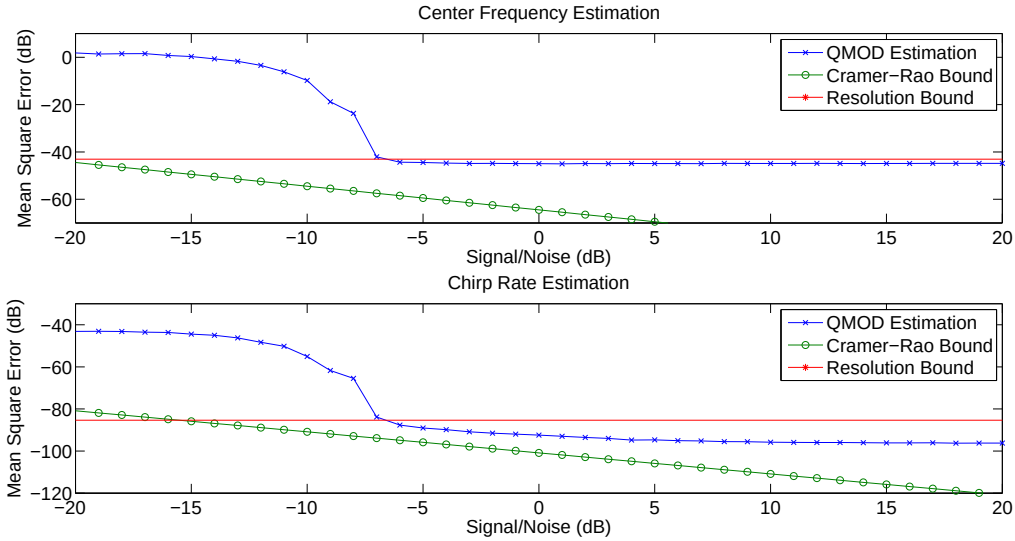

Figure 11: Cross-hairs estimation error: The MSE was calculated at each SNR using 1000 chirps of length N = 256, in the 'safe' range of $|\alpha|(N-1)+|w| = IF < 0.85\pi$. A transform of size NXN was used, refined using minimum norm subspace decomposition and FFT of size R = 4096. Note that the QMOD method produces very less mean square error for both center frequency estimation and chirp rate estimation if they are calculated using cross-hair estimation technique.

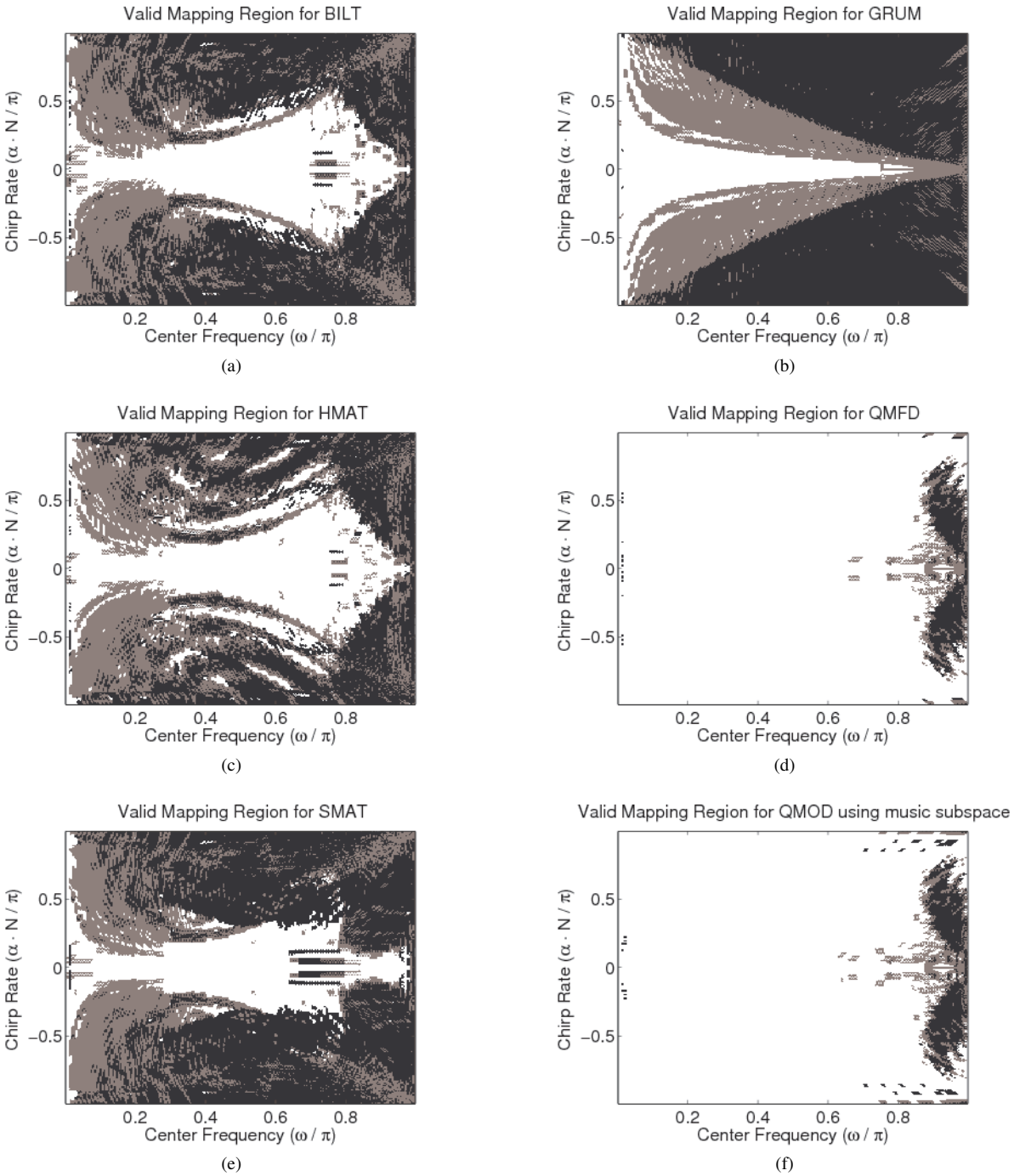

Figure 12: Valid Mapping Regions for N = 256 obtained from (a) Bilinear Transformation Method, (b) Grunbaum Method, (c) Higher order S-matrix Method, (d) QMOD Method and (e) Dickinson-Steiglitz Method (f) QMOD Method using music subspace technique. Figure (a) through (e) are obtained using minimum norm subspace technique. The QMOD method exhibits the largest inverbility region in $\alpha - \omega$ plane. Note that the invertibility region is based on the eigenvector basis not on the subspace decomposition method

.

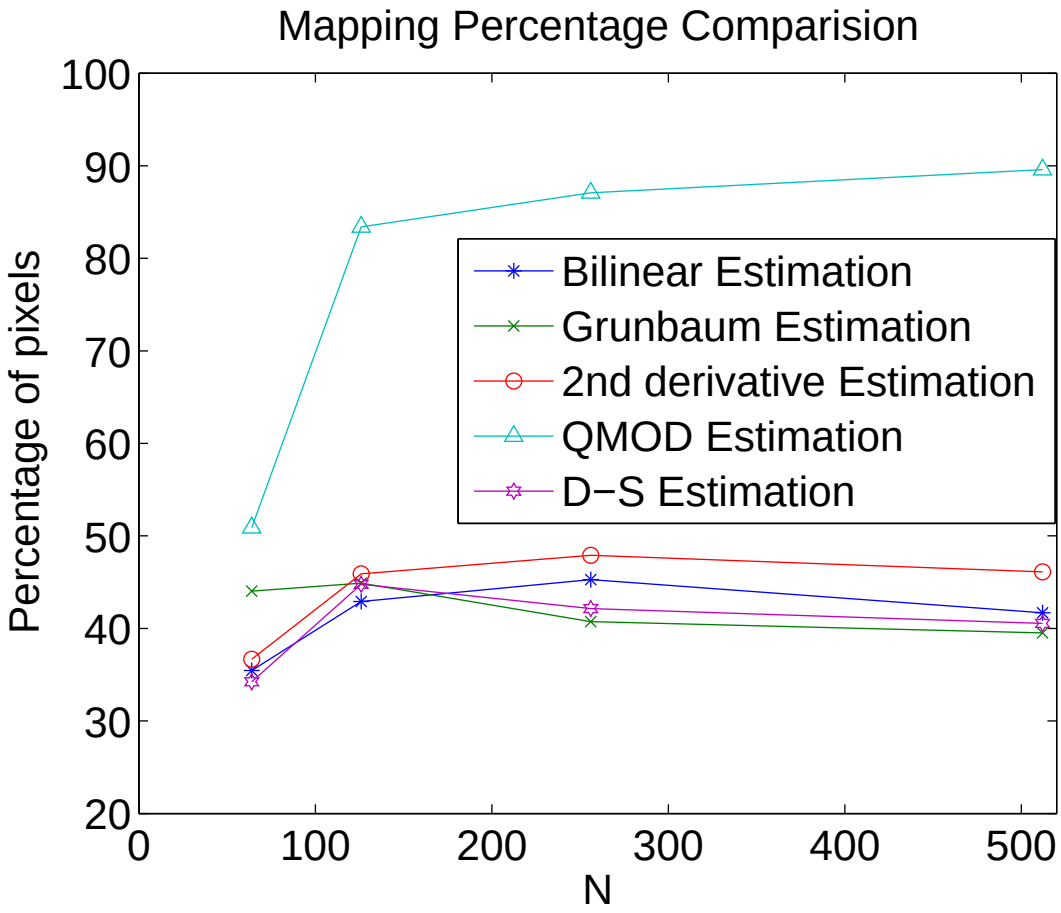

Figure 13: Plot of percentage of pixels in $\alpha - \omega$ plane where both connectivity and adjacency criteria are fulfilled. The QMOD method exhibits a steady increase in invertibility of the peak-to-parameter mapping with increase in N. The QMOD method performs far better than other techniques in terms of invertibility of the peak-to-parameter mapping.

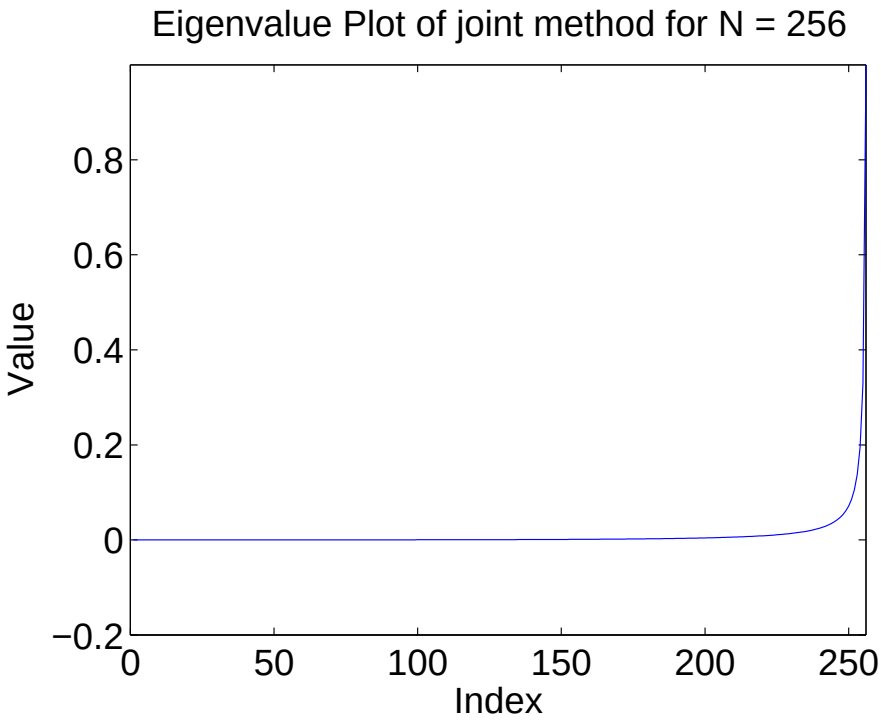

Figure 14: Eigenvalue plot for the joint diagonalization method. This joint diagonalization techniuqe produces nearly 80% linearity in its eigenvalue spectrum.

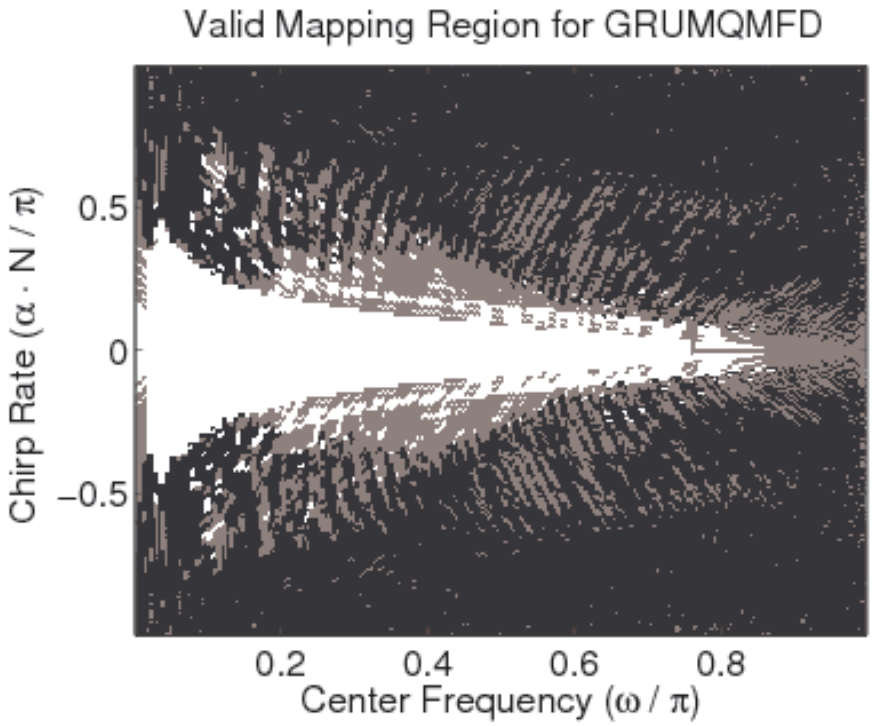

Figure 15: Valid mapping regions for the joint method for N = 256. Note that this combined technique produces a worse invertibility region for the peak-to-parameter mapping than the individual technique.